PIV Measurements of the Flow around Oscillating Cylinders at Low KC Numbers

D. SUMNER, H.B. HEMINGSON, D.M. DEUTSCHER, J.E. BARTH

Department of Mechanical Engineering, University of Saskatchewan

57 Campus Drive, Saskatoon, Saskatchewan, Canada, S7N 5A9, david.sumner@usask.ca

Abstract. The flow around cylinders of circular, square, and diamond cross-section oscillating in quiescent fluid was studied experimentally using particle image velocimetry (PIV). Phase-averaged measurements of the velocity field were obtained at the maximum-amplitude, zero-amplitude, and intermediate positions of the oscillation cycle. The experiments were performed at low Keulegan-Carpenter numbers, from KC = 1 to 3.5, and for moderate Stokes numbers, from β = 250 to 376. Within this range of KC, the flow patterns remained symmetric about either side of the cylinders. For KC = 1, the flow remained close to the surface of the cylinders throughout the cycle. For KC = 1.5 to 3.5, an attached vortex pair formed behind the circular and square cylinders at the maximum-amplitude position. The distinct geometry of the diamond cylinder, with two fixed separation points, led to a unique but still symmetric vortex pattern.

Key words: unsteady flow, bluff body, cylinder, oscillation, particle image velocimetry.

1. Introduction

The flow around a two-dimensional circular cylinder of diameter, D, oscillating sinusoidally from side to side with amplitude, A, and frequency, f (or period, $T = 1/f$), in quiescent fluid of kinematic viscosity, v, can be considered a fundamental problem in unsteady fluid mechanics (Figure 1). The flow is a useful starting point for the study of flow-induced vibrations and has applications in the behaviour of offshore structures in wave motion. The time-dependent cylinder position, $x(t)$, and velocity, $u(t)$, are given by

$$x(t) = A\sin(\omega t) \text{ and} \tag{1}$$

$$u(t) = U_{max}\cos(\omega t), \tag{2}$$

respectively, where t is time, ω ($= 2\pi f$) is the angular frequency, and U_{max} is the maximum cylinder velocity,

$$U_{max} = A\omega = 2\pi Af = 2\pi A/T . \tag{3}$$

Experimental [1, 7, 8, 9, 10, 13, 14] and numerical [3, 12, 15] studies of the oscillating circular cylinder have identified several flow regimes, which are pri-
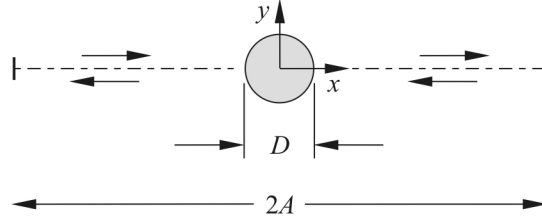
Figure 1. Circular cylinder of diameter, D, oscillating with amplitude, A, in a quiescent fluid.

marily a function of the dimensionless amplitude parameter known as the Keulegan-Carpenter number, KC, where

$$KC = U_{max}T/D = 2\pi A/D. \tag{4}$$

A second influencing parameter is the Reynolds number, Re, which is defined using the maximum cylinder velocity,

$$Re = U_{max}D/\nu = 2\pi ADf/\nu. \tag{5}$$

The dimensionless Stokes number (or reduced frequency), β, is often used instead of the Reynolds number and behaves in a similar manner, where

$$\beta = Re/KC = fD^2/\nu. \tag{6}$$

The number of flow regimes, and the limiting values of KC defining these regimes, are functions of Re or β. For sufficiently high values of β, the flow regime is almost solely determined by KC. The flow patterns are distinguished by the "wake re-encounter" phenomenon, where separated flow and vortices formed and shed by the cylinder during one half cycle return to interact with the cylinder during the next half cycle [5]. For KC $\leq$ 1, the flow does not appreciably separate from the cylinder and the extent of the ambient fluid affected by the moving cylinder is small. For 1 < KC < 4, the flow separates from the cylinder and a symmetric pair of attached vortices forms behind the cylinder during each half cycle. For 4 $\leq$ KC < 8, the attached vortex pair becomes asymmetric. For KC $\geq$ 8, vortex shedding occurs during each half cycle [5, 14].

Similar flow regimes and KC boundaries can be identified for square and diamond-shaped cylinders, as shown in several experimental [1, 8, 9] and numerical [11, 12] studies. For the circular cylinder, the separation points are free to move over large distances during an oscillation cycle [10]. However, for the oscillating square cylinder, the separation points are fixed at the four corners; for the oscillating diamond cylinder, there are only two fixed separation points.

There are relatively few experimental studies of oscillating cylinders which report velocity field measurements [2, 4, 6]. In the present study, particle image velocimetry (PIV) was used to measure the velocity field of oscillating circular,
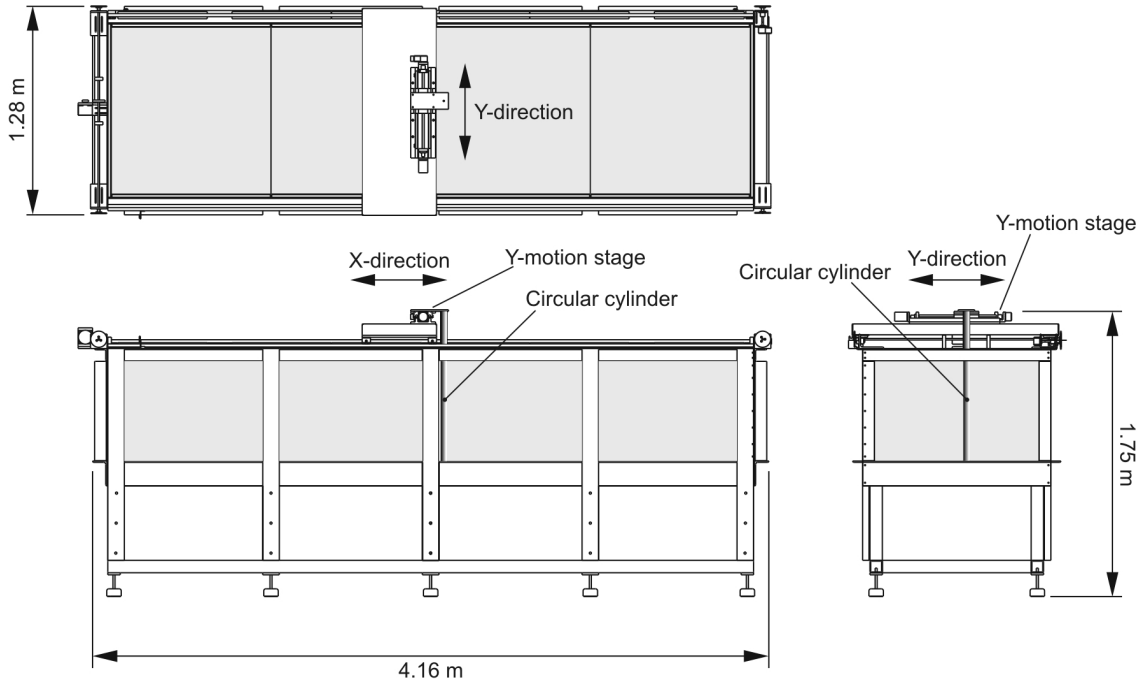
Figure 2. Three-view drawing of the X-Y towing tank, showing the circular cylinder suspended in the water beneath the Y-motion stage.

square and diamond cylinders at low KC numbers. The PIV measurements were phase locked with the cylinder position, at the zero-amplitude (corresponding to dimensionless time $t^* = t/T = 0, 0.5$), maximum-amplitude ($t^* = 0.25, 0.75$), and intermediate positions ($t^* = 0.125, 0.375, 0.625, 0.875$) in the oscillation cycle.

2.   Experimental Approach

The oscillating cylinder experiments were conducted in water in an X-Y towing tank (Figure 2) with internal dimensions of 3.96 m long, 1.03 m wide, and 0.75 m deep. The glass side walls, end walls, and floor of the towing tank give optical access for the PIV system. The primary towing direction (X-direction, 3.5 m of travel) is along the length of the tank, where the main carriage straddles the tank width and moves on two parallel rails. A linear motion stage containing the secondary carriage is mounted on the main carriage for transverse movement across the tank (Y-direction, 260 mm of travel).

   The motion control system for the X-Y towing tank includes a personal computer, a National Instruments (NI) PCI-7344 motion controller card, two Intelligent Motion Systems IM1007 micro-step drivers, and a stepping motor on each axis. Encoders provide closed-loop position feedback. The user interface was developed in the LabVIEW programming language.

   In the present study, only the secondary carriage (Y-direction) was used. A circular or square cylinder of $D = 25.4$ mm (for the square cylinder, D corresponds to the side length) was suspended in the water vertically beneath the Y-

Table 1. Summary of oscillating cylinder experiments.

Cylinder	KC	β	Re	A/D	Cylinder	KC	β	Re	A/D
Circular	1.0	376	376	0.159	Square	2.5	250	625	0.398
Circular	1.5	325	488	0.239	Square	3.0	250	750	0.477
Circular	2.0	250	499	0.318	Square	3.5	250	875	0.557
Circular	2.5	250	625	0.398	Diamond	1.0	374	374	0.159
Circular	3.0	250	751	0.477	Diamond	1.5	325	488	0.239
Circular	3.5	250	875	0.557	Diamond	2.0	251	502	0.318
Square	1.0	375	375	0.159	Diamond	2.5	250	625	0.398
Square	1.5	325	488	0.239	Diamond	3.0	250	751	0.477
Square	2.0	250	500	0.318	Diamond	3.5	250	875	0.557

motion stage (Figure 2). The cylinder aspect ratio ranged from AR = 25.5 to 26.7. The oscillation amplitude ranged from A = 4.04 to 14.15 mm (giving KC = 1 to 3.5). The oscillation frequency ranged from f = 0.38 to 0.60 Hz (giving β = 250 to 376 and Re = 374 to 875); see Table 1.

Velocity field measurements (u and v components, in the x and y directions, respectively) were made with a TSI PIV system. Laser light was supplied by a 120-mJ/pulse dual Nd:YAG laser. The light sheet was located 29.2 cm above the lower end of the cylinder. Images were acquired with a TSI PIVCAM 10-30 (1 Megapixel) camera in a fixed location beneath the tank. The timing was controlled by a TSI LaserPulse synchronizer and Insight 5 software and was phase-locked to a reference signal from the motion control system. The water was seeded with 8-12-µm hollow glass spheres. Image pairs were processed with a single-pass Nyquist grid algorithm, a FFT correlation algorithm, and a Gaussian peak detection algorithm. The interrogation window was 32 × 32 pixels. The field of view was approximately 80 × 80 mm (60 × 60 vectors with 50% overlap) giving a spatial resolution greater than [4] but lower than [6].

For each phase (cylinder position), an ensemble average of 250 instantaneous velocity vector fields was obtained. The cylinder completed at least 50 oscillation cycles before PIV measurements were made, to give sufficient time for the flow patterns to be established. The numerical simulations of [12] showed that at least 15 cycles were needed to reach equilibrium flow behaviour.

3. Results and Discussion

For the range of KC numbers investigated, $1 \le KC \le 3.5$, the flow fields were symmetric about the axis of motion and on opposite ends of the cylinder for subsequent half-cycles, for all three cylinder geometries. Selected results (only vorticity results are presented here) are shown in Figures 3, 4 and 5.

3.1. CIRCULAR CYLINDER

For the oscillating circular cylinder (Figure 3), frame-by-frame analysis of the instantaneous velocity fields did not show any asymmetry on either side of the axis of motion up to KC = 3.5, consistent with [14, 15]. The flow at these KC
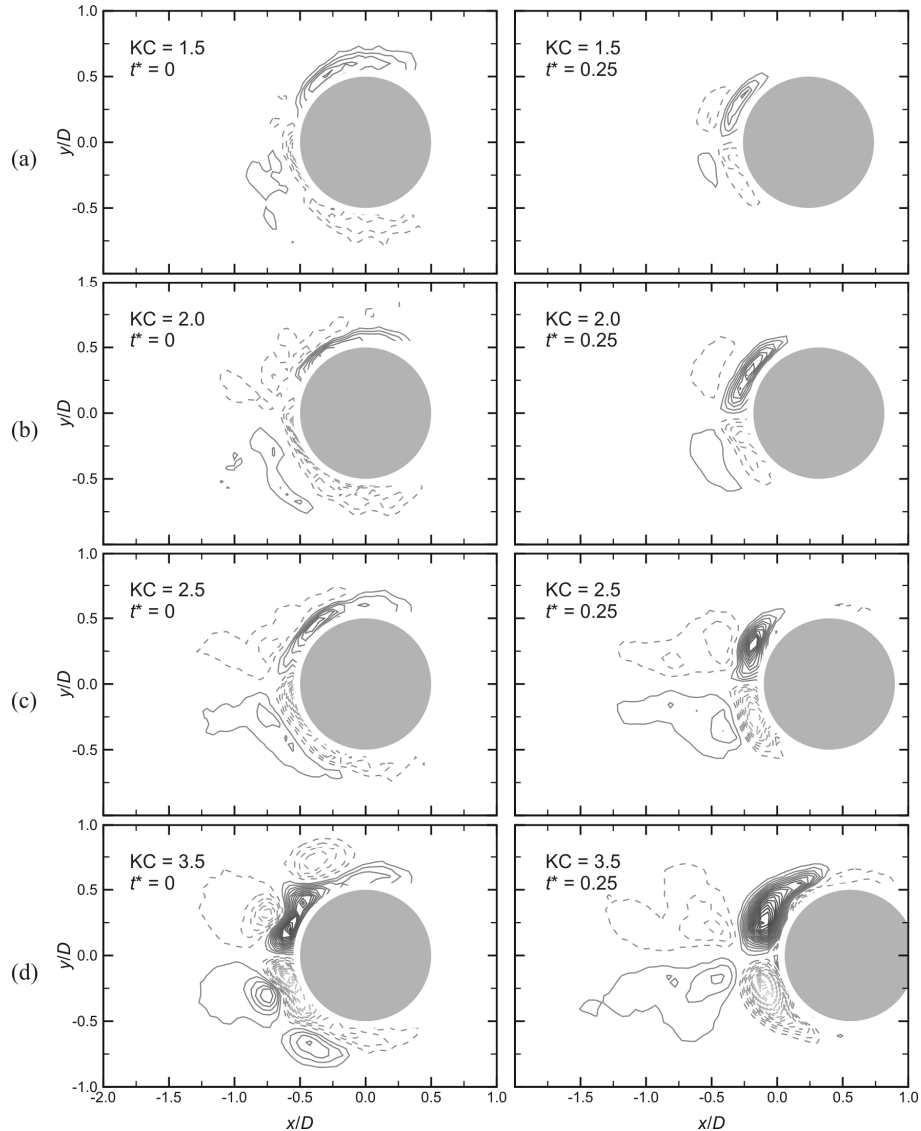
Figure 3. Phase-averaged vorticity fields for an oscillating circular cylinder at the zero- ($t* = 0$) and maximum-amplitude ($t* = 0.25$) positions, cylinder moving to the right: (a) KC = 1.5, $\beta = 325$; (b) KC = 2, $\beta = 250$; (c) KC = 2.5, $\beta = 250$; (d) KC = 3.5, $\beta = 250$. Solid iso-vorticity contour lines represent positive (CCW) vorticity; dashed lines represent negative (CW) vorticity. Minimum vorticity contour of $\omega* = 0.5$, contour increment of $\omega* = 0.5$.

numbers is characterized, for the most part, by the formation and movement of concentrations of vorticity and/or symmetric vortex pairs behind and about the cylinder.

At KC = 1, the fluid is swept symmetrically around the circular cylinder from the front to the rear, the process repeating itself with minimal disturbance to the surrounding fluid as the cylinder reverses direction. The region of disturbed, separated flow is small and remains close to the cylinder surface throughout the range of motion, consistent with [5, 15]. The largest concentrations of vorticity are seen on either side of the cylinder at the zero-amplitude ($t* = 0$) position. As

the cylinder moves toward the maximum-amplitude position ($t^* = 0.25$), these concentrations are swept behind the circular cylinder and weaken.

At KC = 1.5 (Figure 2a), the flow field is generally similar to KC = 1, with the separated flow remaining close to the cylinder throughout the cycle. However, a small, weak attached vortex pair is observed behind the circular cylinder at the maximum-amplitude position ($t^* = 0.25$), which is the primary feature of the flow regime for 1 < KC < 4.

For KC = 2 (Figure 2b), the flow behind the cylinder at maximum amplitude ($t^* = 0.25$) contains a prominent attached symmetric vortex pair, similar to what is observed in the near-wake region of an impulsively started circular cylinder, where each vortex is of similar size and strength but of opposite sign. Behind this vortex pair is weaker detached vortex pair, with vortices of opposite sign to those that are attached. As the cylinder reverses direction ($t^* = 0.375$), the attached vortex pair is now ahead of the moving cylinder, and it quickly diminishes in size and vanishes; this is consistent with the simulations of [3].

The flow is similar for KC = 2.5 (Figure 2c), where a strong attached vortex pair forms at maximum amplitude ($t^* = 0.25$). This is accompanied by the detached vortex pair of opposite sign extending further from the cylinder. As the cylinder reverses direction, the attached vortex pair disappears ($t^* = 0.375$) while the detached vortex pair is split by the approaching cylinder ($t^* = 0.5$). These two concentrations of vorticity are then entrained into the new attached vortex pair that forms behind the cylinder on the opposite side ($t^* = 0.625$).

At KC = 3 (Figure 2d) and 3.5, the attached vortex pair is stronger and more prominent than at KC = 2 and 2.5. The behaviour is characterized by the movement of vortex pairs around the circular cylinder from the front to rear [12, 14]. As the cylinder reverses direction ($t^* = 0.375, 0.5$) the attached vortices no longer disappear. Instead, they detach from the cylinder and sweep around into the new wake that is developing behind the cylinder ($t^* = 0.5, 0.625$). As this happens, they pair up with the developing vortices that will form the attached vortex pair at the next maximum-amplitude position. The swept vortices eventually meet and pair up downstream of the attached vortex pair.

3.2. SQUARE CYLINDER

For the oscillating square cylinder (Figure 4), the four sharp corners lead to well-defined separation points. Vortex formation from the leading corners leads to a wider region of disturbed flow compared to the circular cylinder [9].

For KC = 1 (Figure 4a), the vortex structures that form during the cycle remain close to the cylinder surface. Movement of vorticity along the upper and lower surfaces of the cylinder results in the formation of a vortex pair at each of the rear corners at the maximum-amplitude position ($t^* = 0.25$).

For KC = 1.5 and 2 (Figure 4b), an attached vortex pair forms behind the square cylinder, similar to what is observed for the circular cylinder, and consis-
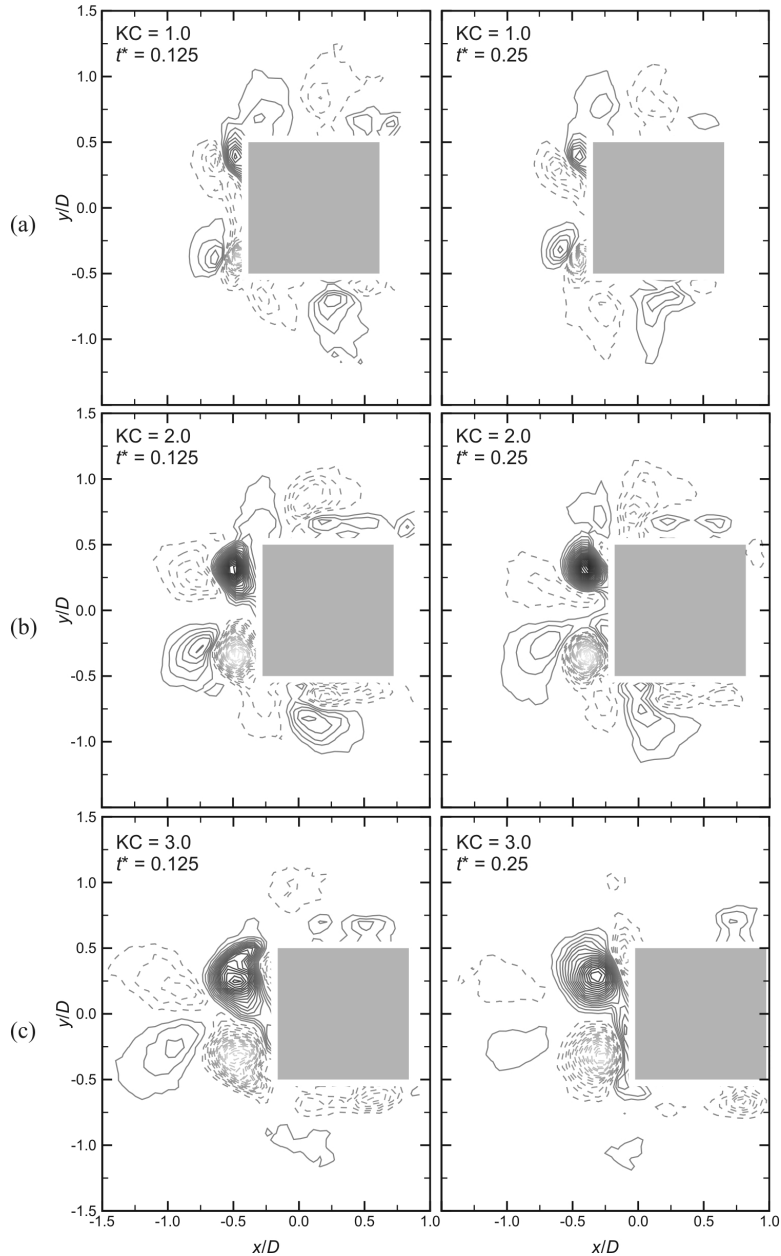
Figure 4. Phase-averaged vorticity fields for an oscillating square cylinder at intermediate- (t^* = 0.125) and maximum-amplitude (t^* = 0.25) positions, cylinder moving to the right: (a) KC = 1, β = 375; (b) KC = 2, β = 250; (c) KC = 3, β = 250. Contour lines as in Figure 3.

tent with [9]. The vortex pair does not meet at the flow centerline; rather, at the maximum-amplitude position (t^* = 0.25), there is an arrangement of four vortices of alternating sign on the rear surface of the cylinder, and another pair of vortices of opposite sign at the rear corners (Figure 4b).

The flow pattern has distinct differences at KC = 3 (Figure 4c) and 3.5 (the flow pattern for KC = 2.5 can be considered transitional). The pairs of vortices at the rear corners are less prominent. Flow separation from the front corners of the square cylinder leads to the formation of small corner vortices. The corner vor-

tices from the previous half cycle enter the wake of the cylinder and form a second, detached vortex pair of opposite sign situated behind the main attached vortex pair (shown for $t^* = 0.125$ in Figure 4c). The detached vortex pair weakens at the maximum-amplitude position ($t^* = 0.25$) and is absent when KC = 3.5.

3.3. DIAMOND CYLINDER

The flow around the oscillating diamond cylinder (Figure 5) is distinct from the circular and square cylinders, being characterized by flow separation and vorticity production at the upper and lower sharp corners. In the direction of motion, the angled flat surfaces meet at the front sharp corner that forms the leading edge. Each flat surface pushes the fluid to the side and some of the fluid flows around the upper and lower corners into the wake. In the base region, the angled flat surfaces meet at the rear sharp corner that forms the trailing edge.

For KC = 1 (Figure 5a), appreciable fluid movement is confined mainly to the regions about the upper and lower corners, where large concentrations of vorticity are produced. The sign of the upper and lower corner vorticity concentrations alternates from one half cycle to the next. During the half cycle, these concentrations of vorticity move behind the diamond cylinder to positions on the angled flat surfaces on the trailing edge. At the maximum-amplitude position ($t^* = 0.25$), an attached pair of opposite-sign vortices has formed on both the upper and lower angled flat surfaces on the rear of the diamond cylinder. Narrow rows of vorticity, resembling free shear layers, extend away from the diamond cylinder parallel to the axis of motion on the upper and lower sides of the flow field.

For KC = 1.5, 2 (Figure 5b), and 2.5, large concentrations of vorticity are produced at the upper and lower sharp corners. These vorticity concentrations are convected into the wake of the diamond cylinder. On the angled flat surfaces at the rear of the cylinder, each pairs up with a vorticity concentration of opposite sign. At the maximum-amplitude position ($t^* = 0.25$), an attached vortex pair has formed on each of the rear angled flat surfaces.

For KC = 3 (Figure 5c) and 3.5, only a single, large attached vortex forms on each of the flat surfaces at the rear of the diamond cylinder. Weaker concentrations of vorticity of opposite sign form further downstream, but are not attached to the flat surfaces (as in the case of KC = 1.5 to 2.5).

4. Conclusions

In the present study, PIV was used to study the velocity and vorticity fields for circular, square and diamond cylinders oscillating in quiescent fluid at low Keulegan-Carpenter numbers (KC = 1 to 3.5) and moderate Stokes numbers ($\beta = 250$ to 376). Phase-averaged velocity and vorticity fields were obtained at the maximum-amplitude, zero-amplitude, and intermediate positions of the oscilla-

tion cycle. The flow patterns remained symmetric about either side of the oscillation axis. For KC = 1, the flow remained close to the cylinder surfaces throughout the oscillation cycle. For KC = 1.5 to 3.5, attached vortex pairs formed behind the cylinders at the maximum-amplitude position. The flow around the diamond cylinder was generally distinct from the circular and square cylinders, which can be attributed, in part, to its different base geometry.

Acknowledgments

References

1. Bearman, P.W., Graham, J.M.R., Obasaju, E.D., and Drossopoulos, G.M., The influence of corner radius on the forces experienced by cylindrical bluff bodies in oscillatory flow. *Appl. Ocean Res.* **6** (1984) 83–89.
2. Dütsch, H., Durst, F., Becker, S., and Lienhart, H., Low-Reynolds-number flow around an oscillating circular cylinder at low Keulegan-Carpenter numbers. *J. Fluid Mech.* **360** (1998) 249–271.
3. Iliadis, G. and Anagnostopoulos, P., Viscous oscillatory flow around a circular cylinder at low Keulegan-Carpenter numbers and frequency parameters. *Int. J. Numer. Meth. Fl.* **26** (1998) 403–442.
4. Lam, K.M. and Dai, G.Q., Formation of vortex street and vortex pair from a circular cylinder oscillating in water. *Exp. Therm. Fluid Sci.* **26** (2002) 901–915.
5. Lin, X.W., Bearman, P.W., and Graham, J.M.R., A numerical study of oscillatory flow about a circular cylinder for low values of beta parameter. *J. Fluid Struct.* **10** (1996) 501–526.
6. Lin, J.C. and Rockwell, D., Quantitative interpretation of vortices from a cylinder oscillating in quiescent fluid. *Exp. Fluids* **23** (1997) 99–104.
7. Obasaju, E.D., Bearman, P.W., and Graham, J.M.R., A study of forces, circulation and vortex patterns around a circular cylinder in oscillating flow. *J. Fluid Mech.* **196** (1988) 467–494.
8. Okajima, A., Matsumoto, T., and Kimura, S., Force measurements and flow visualization of bluff bodies in oscillatory flow. *J. Wind Eng. Ind. Aerod.* **69-71** (1997) 213–228.
9. Okajima, A., Matsumoto, T., and Kimura, S., Force measurements and flow visualization of circular and square cylinders in oscillatory flow. *JSME Int. J. B-Fluid T.* **41** (1998) 796–805.
10. Sarpkaya, T. and Butterworth, W., Separation points on a cylinder in oscillating flow. *J. Offshore Mech. Arct.* **114** (1992) 28–35.
11. Scolan, Y.-M. and Faltinsen, O.M., Numerical studies of separated flow from bodies with sharp corners by the vortex in cell method. *J. Fluid Struct.* **8** (1994) 201–230.
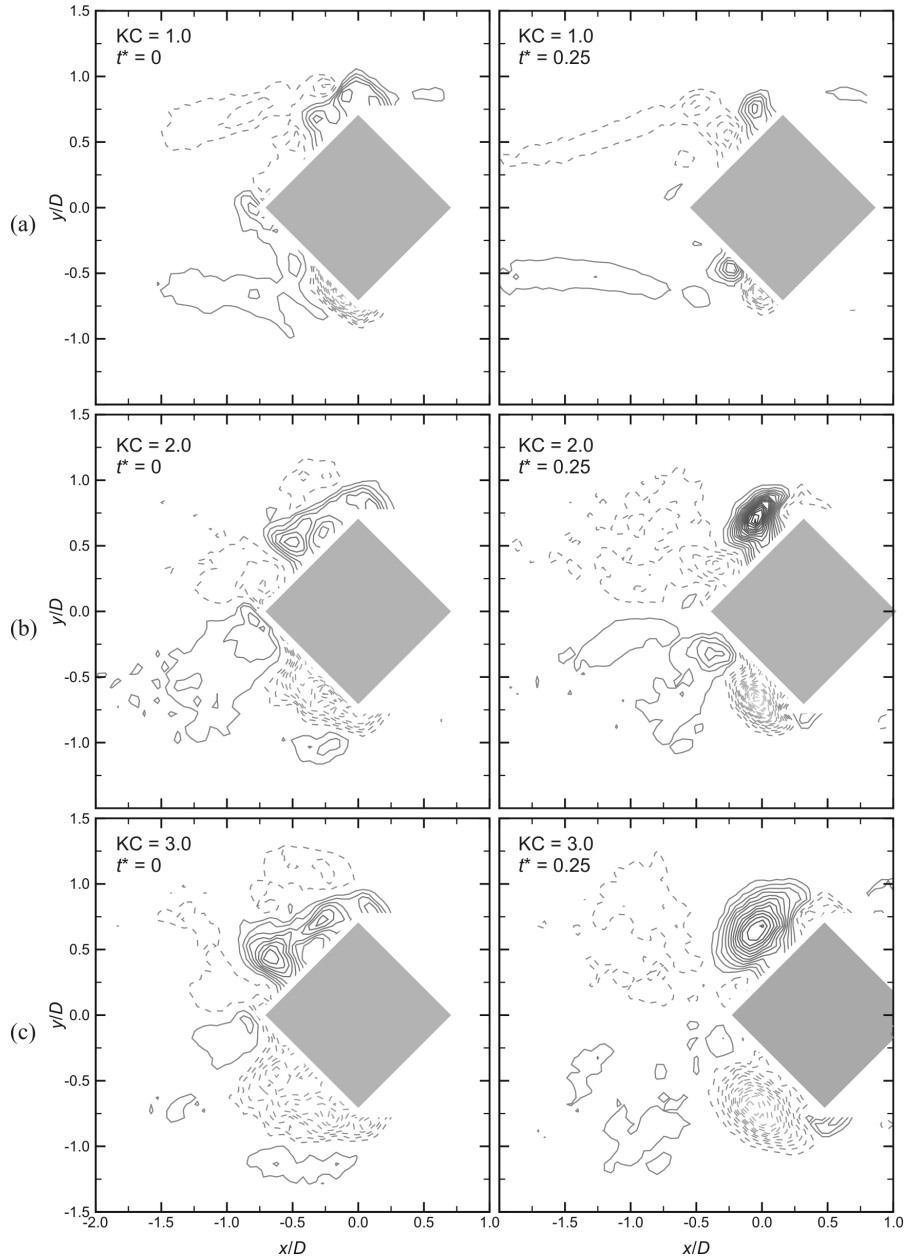
Figure 5. Phase-averaged vorticity fields for an oscillating diamond cylinder at the zero- ($t^* = 0$) and maximum-amplitude ($t^* = 0.25$) positions, cylinder moving to the right: (a) KC = 1, $\beta = 374$; (b) KC = 2, $\beta = 251$; (c) KC = 3, $\beta = 250$. Contour lines as in Figure 3.

12. Smith, P.A. and Stansby, P.K., Viscous oscillatory flow around cylindrical bodies at low Keulegan-Carpenter numbers using the vortex method. *J. Fluid Struct.* **5** (1991) 339–361.

13. Tatsuno, M. and Bearman, P.W., A visual study of the flow around an oscillating circular cylinder at low Keulegan-Carpenter numbers and low Stokes numbers. *J. Fluid Mech.* **211** (1990) 157–182.

14. Williamson, C.H.K., Sinusoidal flow relative to circular cylinders. *J. Fluid Mech.* **155** (1985) 141–174.

15. Zhang, H.-L. and Zhang, X., Flow structure analysis around an oscillating circular cylinder at low KC number: a numerical study. *Comput. Fluids* **26** (1997) 83–106.